AFRL-AFOSR-VA-TR-2022-055

Overcoming the DX Doping Challenge in Ultra Wide Bandgap Semiconductors

Sitar, Zlatko
NORTH CAROLINA STATE UNIVERSITY
2601 WOLF VILLAGE WAY
RALEIGH, NC, 27607
USA

09/16/2021
Final Technical Report

DISTRIBUTION A: Distribution approved for public release.

Air Force Research Laboratory
Air Force Office of Scientific Research
Arlington, Virginia 22203
Air Force Materiel Command

REPORT DOCUMENTATION PAGE

Form Approved
OMB No. 0704-0188

The public reporting burden for this collection of information is estimated to average 1 hour per response, including the time for reviewing instructions, searching existing data sources, gathering and maintaining the data needed, and completing and reviewing the collection of information. Send comments regarding this burden estimate or any other aspect of this collection of information, including suggestions for reducing the burden, to Department of Defense, Washington Headquarters Services, Directorate for Information Operations and Reports (0704-0188), 1215 Jefferson Davis Highway, Suite 1204, Arlington, VA 22202-4302. Respondents should be aware that notwithstanding any other provision of law, no person shall be subject to any penalty for failing to comply with a collection of information if it does not display a currently valid OMB control number.
PLEASE DO NOT RETURN YOUR FORM TO THE ABOVE ADDRESS.

1. REPORT DATE *(DD-MM-YYYY)*	**2. REPORT TYPE**	**3. DATES COVERED** *(From - To)*
16-09-2021	Final	01 Jun 2017 - 31 May 2021

4. TITLE AND SUBTITLE
Overcoming the DX Doping Challenge in Ultra Wide Bandgap Semiconductors

5a. CONTRACT NUMBER

5b. GRANT NUMBER
FA9550-17-1-0225

5c. PROGRAM ELEMENT NUMBER
61102F

6. AUTHOR(S)
Zlatko Sitar

5d. PROJECT NUMBER

5e. TASK NUMBER

5f. WORK UNIT NUMBER

7. PERFORMING ORGANIZATION NAME(S) AND ADDRESS(ES)
NORTH CAROLINA STATE UNIVERSITY
2601 WOLF VILLAGE WAY
RALEIGH, NC 27607
USA

8. PERFORMING ORGANIZATION REPORT NUMBER

9. SPONSORING/MONITORING AGENCY NAME(S) AND ADDRESS(ES)
AF Office of Scientific Research
875 N. Randolph St. Room 3112
Arlington, VA 22203

10. SPONSOR/MONITOR'S ACRONYM(S)
AFRL/AFOSR RTA1

11. SPONSOR/MONITOR'S REPORT NUMBER(S)
AFRL-AFOSR-VA-TR-2022-055

12. DISTRIBUTION/AVAILABILITY STATEMENT
A Distribution Unlimited: PB Public Release

13. SUPPLEMENTARY NOTES

14. ABSTRACT
We demonstrate Si-implanted AlN with high conductivity (>1 Î©-1cm-1) and high carrier concentration (5x1018 cm-3). This was enabled by Si-implantation into AlN with low TDD (<103 cm-2), a non-equilibrium damage recovery and dopant activation annealing process, and in situ suppression of self-compensation during the annealing. Low TDD and active suppression of VAl-nSiAl complexes via defect quasi Fermi level (dQFL) control enabled low compensation, while low-temperature, non-equilibrium annealing maintained the desired shallow donor state with an ionization energy of ~70 meV. The achieved n-type conductivity and carrier concentration are over one order of magnitude higher than reported thus far and present a major technological breakthrough in doping of AlN. Contrary to the established understanding, we find that Ge in AlGaN does not suffer from the DX transition; instead, it undergoes a shallow donor (30 meV) to deep donor (150 meV) transition at ~50% Al content in the alloy. This finding is of profound technological importance as it removes fundamental doping limitations in AlGaN and AlN imposed by the presumed DX-1 acceptor state.

15. SUBJECT TERMS

16. SECURITY CLASSIFICATION OF:			**17. LIMITATION OF ABSTRACT**	**18. NUMBER OF PAGES**	**19a. NAME OF RESPONSIBLE PERSON**
a. REPORT	**b. ABSTRACT**	**c. THIS PAGE**			KENNETH GORETTA
U	U	U	UU	20	**19b. TELEPHONE NUMBER** *(Include area code)* 426-7349

Standard Form 298 (Rev.8/98)
Prescribed by ANSI Std. Z39.18

Contract: FA9550-17-1-0225

Overcoming the DX doping challenge in ultra-wide bandgap semiconductors

Final Report (2021)

by

Zlatko Sitar, Douglas Irving, and James LeBeau

Department of Materials Science & Engineering

North Carolina State University, Raleigh, NC 27695-7907

Program Manager:

Dr. Kenneth Goretta,

Air Force Office of Scientific Research

DISTRIBUTION A: Distribution approved for public release.

1 Challenge and significance of the opportunity

For the AlN-based power electronics to become a reality, controllable doping of ultra-wide bandgap AlGaN alloys is essential. Presumable DX transitions have hindered this progress. Therefore, this basic science program aims to understand the shallow donor to DX transition and to develop practical strategies to suppress or even eliminate its occurrence in AlN. Although the model material is AlN, the understanding and possible solutions brought forth by this program are generally applicable to other materials.

Theory and experiment find that Si incorporates in GaN and lower Al-content AlGaN as a shallow donor with an ionization energy of ~20 meV. This results in it being almost fully ionized at room temperature and tailorable electron concentrations and mobilities are achievable. In AlN, this is not the case. All the donor dopants that were shallow at low Al-content now have a significant, beyond expected, increase in their ionization energy and can no longer be considered as hydrogenic-like dopants in AlN. The transition from a shallow donor (~20 meV) to deep donor/acceptor (~250-310 meV) as a function of Al content for Si-doped AlGaN alloys has been measured by our team and other researchers around the world. The abrupt transition from a shallow to deep donor arises not only from an increase in the energy gap but also from the emergence of an increasingly favorable geometry for Si to reside off the substitutional site in AlN. This shift to an off-lattice site position is accompanied by a local trapping of an electron (making it an acceptor), which effectively pins the Fermi level farther below the conduction band. This displacement is referred to as a DX transition and the off-lattice site coordinates have been determined by density functional theory (DFT) calculations. While theory predicts the presence of this defect, experimental confirmation has been limited to indirect measurements (electrical and PL). With new capabilities in microscopy, opportunities arise to directly observe and study this defect in real space, which provides critical feedback to understand governing mechanisms that need to be understood for its control and elimination. This project investigates the most common donor dopants that are known to be shallow in GaN and transition to deep donors in AlN, i.e., Si, Ge, and O. The onset of the formation of DX centers is studied in a series of AlGaN alloys with increasing Al content up to pure AlN.

The working hypothesis is that the DX formation is likely influenced by a number of structural and electronic factors that include lattice parameter, bandgap, depth of the valence band, and local chemistry. Advanced first principles calculations that use state-of-the-art hybrid exchange correlation functionals are being implemented to determine important contributors to DX formation and how DX formation changes as a function of the above factors. The influence of local chemistry and variations in it is a critical factor to explore, however, full and independent exploration by advanced first principles methods alone remains impractical. We couple the theory with accurate and precise STEM measurements to provide a perspective on the local chemical environment, which provide a critical feedback loop to facilitate this investigation. This is enabled by our ability to grow low dislocation density ($<10^3$ cm^{-2}) AlGaN and AlN and to control formation of unwanted point defects via Fermi level control (FLC). One important control parameter leveraged to suppress or activate DX formation is pseudomorphic strain.

1.1 Proposed theoretical and experimental tasks:

1. Prediction of point defect properties
    a. Prediction of defect formation energies
    b. Thermodynamic transition levels
    c. Calculation of expected optical signatures of point defects
2. Growth of AlGaN, doping, and strain control
    a. Growth of Si-, and Ge-doped AlN and Al-rich AlGaN layers
    b. Development of defect control schemes
    c. Growth of thick AlN and Al-rich AlGaN
    d. Structural optical and electrical characterization
3. Advanced electron microscopy of point defects
    a. Scanning transmission electron microscopy (STEM)
    b. Electron energy loss spectroscopy

DISTRIBUTION A: Distribution approved for public release.

2 Current Results

2.1 High n-type Conductivity and carrier concentration in Si-implanted AlN

Background

Aluminum Nitride (AlN) provides an attractive opportunity for the development of next generation power electronic and deep-UV optoelectronic devices due to its large bandgap of 6.1 eV, Schottky barriers > 2 eV and breakdown field greater than 15 $MVcm^{-1}$.[1–5] In order to achieve highly conducting regions for optoelectronics and low doped drift regions for power electronics, doping and compensation must be controlled over several orders of magnitude. However, the achievable free electron concentration in homoepitaxial Si-doped AlN is currently limited to concentrations $<10^{16}$ cm^{-3} at room temperature.[6,7] The carrier concentration is limited partly by compensation by high threading dislocation densities (TDD)[8,9] – AlN films are typically grown on foreign substrates (e.g., sapphire or SiC) with TDD ≥ 10^8 cm^{-2},[10–13] self-compensating vacancy-Si complexes,[9,14] and the formation of a Si DX center accompanied by high activation energy.[6,15,16] Consequently, obtaining highly conducting AlN requires reducing TDD, vacancy complexes, and addressing the formation of the DX center.

AlN films grown by MOCVD on AlN single crystal substrates have been shown to have TDD $<10^3$ cm^{-2}, making the TDD-related compensation negligible.[17] As a recent breakthrough, we have demonstrated that ion implanted Si can remain in the shallow donor state ($d^{0/+}$), with an ionization energy of ~70 meV, rather than relaxing into the deep DX state after damage recovery and dopant activation annealing. This was realized by employing a relatively low annealing temperature (1200°C) to recover the lattice damage, preventing the system from reaching thermodynamic equilibrium and forming energetically favorable deep DX^- acceptor state. However, utilizing higher annealing temperatures and driving the system closer to the equilibrium, resulted in the DX formation and low conductivities, similar those observed for epitaxially doped AlN.[18,19] However, similar to doping during the epitaxial growth, damage recovery and dopant activation annealing process led to high self-compensation, resulting in over an order of magnitude lower conductivity than expected based on the low ionization energy.[18] Hence, controlling the formation of these compensating point defects seems to be the last obstacle in attaining higher free electron concentrations in Si-doped AlN.

In this work, we expand on our previous achievement of shallow (~70 meV) Si doping in low TDD AlN by ion implantation where we showed that ion implantation, as a non-equilibrium process, may provide an avenue to manage the population distribution between the two possible Si states in AlN: a shallow donor and a deep acceptor.[18] In current work, we implement *in situ* control of point defects to suppress self-compensation during the recovery and activation annealing process. The non-equilibrium annealing process in combination with *in situ* point defect control enabled us to achieve more than one order of magnitude higher free carrier concentration than possible before.

In general, the concentration of a point defect that readily incorporates into a crystal depends upon its formation energy, which can be expressed as:[23]

$$E^f(X^q) = E_{ref}(X^q) - \sum_j n_j \mu_j + q(E_F + E_V), \qquad (1)$$

where E_{ref} is the free energy of a crystal with a single defect referenced to the free energy of an ideal crystal, n_j is the number of atoms of the jth-type exchanged with the reservoir to form the defect, μ_j is the associated chemical potential, and E_F is the Fermi energy referenced with respect to the valence band maximum, E_V. From this relationship, there are two paths by which defect incorporation can be controlled: (1) chemical potential, wherein one controls process conditions[24–29] in order to influence corresponding impurity or host chemical potentials to lower the overall defect formation energy,[30,31] and (2) defect Quasi Fermi Level (dQFL), where QFL associated with each defect is modified by introducing excess minority carriers into the system during the process,[32–39] which increases defect's formation energy and decreases its population. A comprehensive study and theoretical framework for the latter approach can be found elsewhere.[32] While we have demonstrated dQFL for epitaxial growth, we hypothesize that the same approach, i.e., generation

DISTRIBUTION A: Distribution approved for public release.

of minority carriers by above bandgap illumination, can be as effective in the damage recovery and dopant activation annealing process.

Experimental

Low dislocation density ($<10^3$ cm^{-2}) AlN single crystal substrates processed from AlN boules grown by physical vapor transport were used in this study.[40–42] AlN homoepitaxial films were grown via metal organic chemical vapor deposition (MOCVD) at a temperature of 1100°C and a total pressure of 20 Torr. The V/III ratio of 1000 was established by flowing 8.4 μmol/min of trimethylaluminum (TMA) and 0.3 slm of ammonia (NH_3) under a total flow rate of 10 slm with hydrogen as a diluent gas. Further details pertaining to AlN homoepitaxial growth are described elsewhere.[43] Si was then implanted into the homoepitaxial AlN film at room temperature with a dose of 1×10^{14} atoms/cm^2 and an acceleration voltage of 100 keV. The AlN films were implanted with a tilt angle of 7° to reduce the effects of channeling during ion implantation.[18]

The optical properties of the AlN films were characterized by photoluminescence spectroscopy (PL) at room temperature using a 193 nm ArF excimer laser with pulse width of 5 ns with a repetition rate of 100 Hz and power density ~5 kW/cm^2. Optical spectra were dispersed in a Princeton Instruments Acton SP2750 0.75 m high-resolution spectrograph using a 3200 grooves/mm optical grating and detected using a PIXIS: 2KBUV Peltier-cooled charge-coupled device camera.

Post-implantation annealing was performed at 1200°C for 120 minutes in a nitrogen atmosphere and a pressure of 100 Torr. Above bandgap UV-illumination during the annealing was implemented by a Hg-Xe lamp (Oriel 6293) with a measured power density of 1 W/cm^2. V/Al/Ni/Au (30/100/70/70 nm) contacts[44,45] in the van der Pauw geometry were deposited onto the surface of samples by electron beam evaporation as described elsewhere.[18] The electrical contacts were annealed via rapid thermal annealing at 850°C for 60 seconds in nitrogen. The carrier type, free electron concentration, and electron mobility were determined by an 8400 series LakeShore AC/DC Hall measurement system performed at elevated temperatures (>400°C). The AC Hall measurements were performed using a magnetic field and excitation frequency of ~0.62 T and 100 mHz, respectively. Temperature-dependent (300-725 K) conductivity measurements were obtained using Ecopia HMS-5500 and contacts in the van der Pauw configuration.

Results and discussion

It was previously reported that annealing of Si-doped AlN at a temperature of 1200°C for implantation damage recovery led to a lower donor ionization energy (E_i ~ 70 meV), with only the shallow donor state $d^{0/+}$ observed, suggesting that the deep DX formation was inhibited.[18] Despite this lower ionization energy and approximately one order of magnitude increase in conductivity at room temperature compared to epitaxially doped AlN:Si, significant compensation was observed, which resulted in much lower electrical conductivity than expected from the low ionization energy. The presence of compensating point defects after the damage recovery and dopant activation process was confirmed by the room temperature PL, showing broad midgap luminescence peaks associated with V_{Al}-nSi_{Al}.[46–48] Similar midgap luminescence and compensation were observed in epitaxially-doped films. We demonstrated more than one order of magnitude reduction in these compensating defects by active point defect control during the growth via minority carrier generation.[32] A similar process utilizing the above bandgap illumination was applied here during the post-implantation annealing. Figure 1 shows midgap luminescence spectra for Si-implanted AlN samples annealed under dark (red) and illuminated (blue) conditions. A significant (more than one order of magnitude) reduction in the midgap luminescence is observed for the UV-annealed samples in comparison to the annealing under dark conditions, suggests a significant suppression of the V_{Al}-nSi_{Al}-related point defects, which have been identified as compensators in Si-doped AlN.[48]

DISTRIBUTION A: Distribution approved for public release.

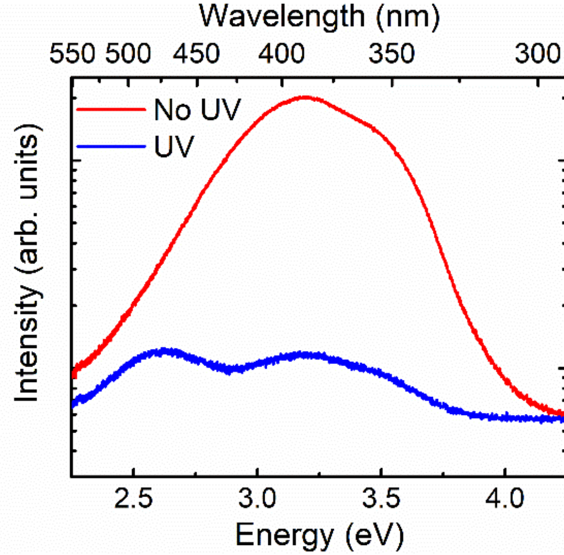

Figure 1. Room temperature photoluminescence spectra for Si-implanted AlN annealed without (red) and with (blue) UV illumination, showing more than one order of magnitude reduction in V_{Al}-nSi_{Al}-related point defects. The spectra were normalized with respect to the band edge luminescence to facilitate direct comparison of the midgap luminescence peaks.

Identifying the main point defects associated with the deep luminescence allows for a prediction of their corresponding decrease based on the dQFL control framework. The procedure to determine the expected decrease in defect concentration for a specified defect at a given illumination intensity is described in detail elsewhere.[32,49] For the estimation, V_{Al}-2Si_{Al} point defects at specific charge states consistent with the measured midgap luminescence spectra were considered.[47,48,50] Using the Varshni equation and the fitting parameters for AlN,[51] we estimate the bandgap of AlN at the annealing temperature (1200°C) to be ~4.9 eV. The experimental work of Reddy et al. shows that the Fermi level for AlN is pinned at ~2.7 eV below the conduction band minimum. Assuming that the barrier height scales with bandgap,[52] we estimate a barrier height of ~2.2 eV at the annealing temperature,[53] which estimates the Fermi level at the annealing temperature of ~2.7 eV above the valence band. Using the estimated Fermi level, a process efficiency of ~90% and a reduction in compensating defect population of around an order of magnitude is expected for samples annealed with the above bandgap illumination as compared to the samples annealed under dark conditions. This estimate roughly corresponds with the observed midgap PL intensity decrease in Figure 1.

Electrical conductivity as a function of temperature for Si-implanted AlN annealed with and without above bandgap illumination is shown in Figure 2. Interestingly, the sample annealed with UV-illumination without reaching equilibrium conditions (1200°C, blue) exhibited a similar slope to the sample annealed without dQFL control (red) but showed about 30-times higher conductivity across the whole temperature range. This inferred that the shallow donor (E_i ~ 70 meV) state was maintained and was determined by the process kinetics rather than illumination. For comparison, the conductivity data for Si-implanted AlN samples annealed at higher temperatures (1400°C and 1500°C) under dark conditions show a much higher ionization energy (E_i ~ 290 meV),[18] comparable to the ionization energy reported for the epitaxially-doped AlN. The ~30-fold increase in conductivity is consistent with the predictions of the dQFL model and the observed reduction in compensator-related midgap photoluminescence intensity.

To estimate the compensation ratio (N_a/N_d) for the two annealing conditions, the conductivity,

$$\sigma = ne\mu, \tag{2}$$

can be used, where n is the number of free electrons, e is the electron charge, and μ is the electron mobility. Since the conductivity change with temperature in semiconductors is dominated by the change in free

DISTRIBUTION A: Distribution approved for public release.

carrier concentration, a charge balance model that relates free carriers with temperature, can be expressed by the following equation:

$$n = \frac{1}{2}\left[-\left(N_a + \frac{1}{g}N_C \exp\left(-\frac{\Delta E_i}{k_B T}\right)\right) + \sqrt{\left(N_a + \frac{1}{g}N_C \exp\left(-\frac{\Delta E_i}{k_B T}\right)\right)^2 + \frac{4}{g}N_C(N_d - N_a)\exp\left(-\frac{\Delta E_i}{k_B T}\right)}\right], \quad (3)$$

where N_a and N_d are the acceptor and donor concentrations, respectively, N_C is the density of states in the conduction band, g is the charge degeneracy factor, T is the temperature, E_i is the ionization energy (70 meV), and k_B is the Boltzmann's constant. The compensation ratios for the samples annealed under dark and illuminated conditions were calculated by fitting the Equation 3 as 0.9 and 0.2, respectively. The obtained reduction in compensation is again consistent with the predicted value, PL results, and increase in conductivity.

The carrier type was confirmed to be *n*-type via the hot probe and AC Hall measurements. The Gaussian implants with carrier concentration and mobility varying with depth introduced difficulties in achieving reliable low temperature Hall measurements, which requiring uniform profiles and properties. However, at temperatures above 400°C, reproducible Hall measurements were obtained, and the measured free electron concentration and mobility were ~$5\text{x}10^{18}$ cm^{-3} and ~1 cm^2/Vs, respectively, assuming uniform properties over a thickness of 200 nm. Hence, the measured sheet carrier concentration of 1×10^{14} cm^{-2} for the sample with dQFL was comparable to the original Si dose implanted into the film, indicating that nearly all of the implanted Si atoms occupied their corresponding substitutional lattice sites and contributed free carriers, i.e., the samples showed high activation and low compensation. The sample annealed without dQFL had approximately one order of magnitude lower sheet carrier concentration ~10^{13} cm^{-2} at a similar mobility.[18] This highlights the utility of dQFL control and its ability to significantly reduce compensation during the post implantation damage recovery and activation annealing process. Although a high conductivity exceeding 1 $\Omega^{-1}\text{cm}^{-1}$ at room temperature was demonstrated in AlN by ion implantation, the measured carrier mobility was about 100-times lower than what can be achieved in the epitaxial doping despite low compensation ratio. This phenomenon requires further investigation.

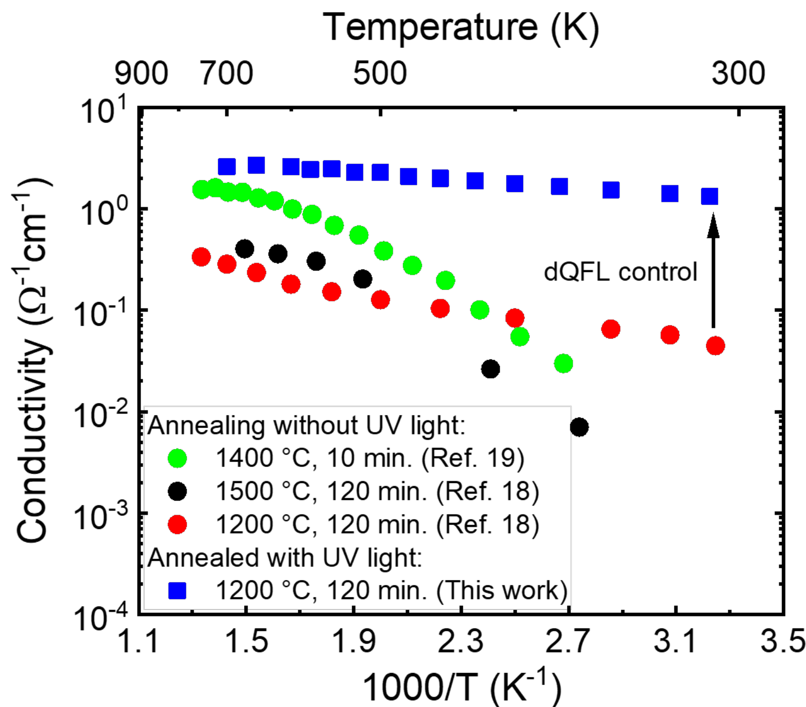

Figure 2. Temperature dependent conductivities for Si implanted AlN samples annealed without UV light: 1400°C for 10 minutes (green circles)[19], 1500°C for 120 minutes (black circles)[18], and 1200°C for 120 minutes (red circles)[18]; and

DISTRIBUTION A: Distribution approved for public release.

the sample annealed with UV light 1200°C for 120 minutes (blue squares).

Conclusions

In conclusion, we have demonstrated a viable process for achieving high sheet conductance and high free carrier concentration in homoepitaxially-grown, Si-implanted AlN. This was enabled by three key process advancements: (1) growth of AlN with TDD <10^3 cm^{-2}, (2) maintaining the Si dopant in a shallow state by a non-equilibrium annealing process, and (3) suppressing self-compensation via V_{Al}-nSi_{Al} complexes by dQFL control. The low ionization energy coupled with low compensation allowed for nearly complete Si ionization at moderate temperatures. A room temperature conductivity >1 $\Omega^{-1}cm^{-1}$ and free carrier concentration as high as $5x10^{18}$ cm^{-3} were achieved.

References

1 H. Angerer, D. Brunner, F. Freudenberg, O. Ambacher, M. Stutzmann, R. Höpler, T. Metzger, E. Born, G. Dollinger, A. Bergmaier, S. Karsch, and H.-J. Körner, Appl. Phys. Lett. 71, 1504 (1997).

2 Q. Guo and A. Yoshida, Jpn. J. Appl. Phys. 33, 2453 (1994).

3 T.L. Chu and R.W. Kelm, J. Electrochem. Soc. 122, 995 (1975).

4 T. Kinoshita, T. Nagashima, T. Obata, S. Takashima, R. Yamamoto, R. Togashi, Y. Kumagai, R. Schlesser, R. Collazo, A. Koukitu, and Z. Sitar, Appl. Phys. Express 8, 061003 (2015).

5 P. Reddy, I. Bryan, Z. Bryan, J. Tweedie, R. Kirste, R. Collazo, and Z. Sitar, J. Appl. Phys. 116, 194503 (2014).

6 R. Zeisel, M.W. Bayerl, S.T.B. Goennenwein, R. Dimitrov, O. Ambacher, M.S. Brandt, and M. Stutzmann, Phys. Rev. B 61, R16283 (2000).

7 Y. Taniyasu, M. Kasu, and T. Makimoto, Appl. Phys. Lett. 85, 4672 (2004).

8 E.C.H. Kyle, S.W. Kaun, P.G. Burke, F. Wu, Y.-R. Wu, and J.S. Speck, J. Appl. Phys. 115, 193702 (2014).

9 I. Bryan, Z. Bryan, S. Washiyama, P. Reddy, B. Gaddy, B. Sarkar, M.H. Breckenridge, Q. Guo, M. Bobea, J. Tweedie, S. Mita, D. Irving, R. Collazo, and Z. Sitar, Appl. Phys. Lett. 112, 062102 (2018).

10 K. Nakano, M. Imura, G. Narita, T. Kitano, Y. Hirose, N. Fujimoto, N. Okada, T. Kawashima, K. Iida, K. Balakrishnan, M. Tsuda, M. Iwaya, S. Kamiyama, H. Amano, and I. Akasaki, Phys. Status Solidi A 203, 1632 (2006).

11 H. Hirayama, S. Fujikawa, N. Noguchi, J. Norimatsu, T. Takano, K. Tsubaki, and N. Kamata, Phys. Status Solidi A 206, 1176 (2009).

12 J. Bai, M. Dudley, W.H. Sun, H.M. Wang, and M.A. Khan, Appl. Phys. Lett. 88, 051903 (2006).

13 H. Miyake, G. Nishio, S. Suzuki, K. Hiramatsu, H. Fukuyama, J. Kaur, and N. Kuwano, Appl. Phys. Express 9, 025501 (2016).

14 S.F. Chichibu, H. Miyake, Y. Ishikawa, M. Tashiro, T. Ohtomo, K. Furusawa, K. Hazu, K. Hiramatsu, and A. Uedono, J. Appl. Phys. 113, 213506 (2013).

15 M. Feneberg, B. Neuschl, K. Thonke, R. Collazo, A. Rice, Z. Sitar, R. Dalmau, J. Xie, S. Mita, and R. Goldhahn, Phys. Status Solidi A 208, 1520 (2011).

16 R. Collazo, S. Mita, J. Xie, A. Rice, J. Tweedie, R. Dalmau, and Z. Sitar, Phys. Status Solidi C 8, 2031 (2011).

17 R. Dalmau, B. Moody, R. Schlesser, S. Mita, J. Xie, M. Feneberg, B. Neuschl, K. Thonke, R. Collazo, A. Rice, J. Tweedie, and Z. Sitar, J. Electrochem. Soc. 158, H530 (2011).

18 M. H. Breckenridge, Q. Guo, A. Klump, B. Sarkar, Y. Guan, J. Tweedie, R. Kirste, S. Mita, P. Reddy, R. Collazo, and Z. Sitar, Appl. Phys. Lett. 116, 172103 (2020).

19 M. Kanechika and T. Kachi, Appl. Phys. Lett. 88, 202106 (2006).

20 I. Bryan, Z. Bryan, S. Washiyama, P. Reddy, B. Gaddy, B. Sarkar, M. Hayden Breckenridge, Q. Guo, M. Bobea, J. Tweedie, S. Mita, D. Irving, R. Collazo, and Z. Sitar, Appl. Phys. Lett. 112, 062102 (2018).

21 R. Collazo, J. Xie, B.E. Gaddy, Z. Bryan, R. Kirste, M. Hoffmann, R. Dalmau, B. Moody, Y. Kumagai, T. Nagashima, Y. Kubota, T. Kinoshita, A. Koukitu, D.L. Irving, and Z. Sitar, Appl. Phys. Lett. 100, 191914 (2012).

22 I. Bryan, Z. Bryan, M. Bobea, L. Hussey, R. Kirste, R. Collazo, and Z. Sitar, J. Appl. Phys. 116, 133517 (2014).

23 C.G.V. de Walle and J. Neugebauer, J. Appl. Phys. 95, 3851 (2004).

24 S. Mita, R. Collazo, A. Rice, R.F. Dalmau, and Z. Sitar, J. Appl. Phys. 104, 013521 (2008).

DISTRIBUTION A: Distribution approved for public release.

25 F. Mehnke, X.T. Trinh, H. Pingel, T. Wernicke, E. Janzén, N.T. Son, and M. Kneissl, J. Appl. Phys. 120, 145702 (2016).

26 F. Kaess, S. Mita, J. Xie, P. Reddy, A. Klump, L.H. Hernandez-Balderrama, S. Washiyama, A. Franke, R. Kirste, A. Hoffmann, R. Collazo, and Z. Sitar, J. Appl. Phys. 120, 105701 (2016).

27 Y. Cao, R. Chu, R. Li, M. Chen, R. Chang, and B. Hughes, Appl. Phys. Lett. 108, 062103 (2016).

28 N.A. Fichtenbaum, T.E. Mates, S. Keller, S.P. DenBaars, and U.K. Mishra, J. Cryst. Growth 310, 1124 (2008).

29 A. Saxler, D. Walker, P. Kung, X. Zhang, M. Razeghi, J. Solomon, W.C. Mitchel, and H.R. Vydyanath, Appl. Phys. Lett. 71, 3272 (1997).

30 P. Reddy, S. Washiyama, F. Kaess, R. Kirste, S. Mita, R. Collazo, and Z. Sitar, J. Appl. Phys. 122, 245702 (2017).

31 S. Washiyama, P. Reddy, B. Sarkar, M.H. Breckenridge, Q. Guo, P. Bagheri, A. Klump, R. Kirste, J. Tweedie, S. Mita, Z. Sitar, and R. Collazo, J. Appl. Phys. 127, 105702 (2020).

32 P. Reddy, M.P. Hoffmann, F. Kaess, Z. Bryan, I. Bryan, M. Bobea, A. Klump, J. Tweedie, R. Kirste, S. Mita, M. Gerhold, R. Collazo, and Z. Sitar, J. Appl. Phys. 120, 185704 (2016).

33 K. Alberi and M.A. Scarpulla, Sci. Rep. 6, 27954 (2016).

34 Z. Bryan, M. Hoffmann, J. Tweedie, R. Kirste, G. Callsen, I. Bryan, A. Rice, M. Bobea, S. Mita, J. Xie, Z. Sitar, and R. Collazo, J. Electron. Mater. 42, 815 (2012).

35 Z. Bryan, I. Bryan, B.E. Gaddy, P. Reddy, L. Hussey, M. Bobea, W. Guo, M. Hoffmann, R. Kirste, J. Tweedie, M. Gerhold, D.L. Irving, Z. Sitar, and R. Collazo, Appl. Phys. Lett. 105, 222101 (2014).

36 M.P. Hoffmann, J. Tweedie, R. Kirste, Z. Bryan, I. Bryan, M. Gerhold, Z. Sitar, and R. Collazo, SPIE Proc. 8986, 89860T (2014).

37 Hoffmann, Marc Patrick, Polarity Control and Doping in Aluminum Gallium Nitride, Technische Universität Berlin, 2013.

38 James S. Tweedie, X-Ray Characterization and Defect Control of III-Nitrides., North Carolina State University, 2012.

39 M. Ichimura, T. Wada, S. Fujita, and S. Fujita, Jpn. J. Appl. Phys. 30, 3475 (1991).

40 Z.G. Herro, D. Zhuang, R. Schlesser, R. Collazo, and Z. Sitar, J. Cryst. Growth 286, 205 (2006).

41 D. Zhuang, Z.G. Herro, R. Schlesser, and Z. Sitar, J. Cryst. Growth 287, 372 (2006).

42 P. Lu, R. Collazo, R.F. Dalmau, G. Durkaya, N. Dietz, B. Raghothamachar, M. Dudley, and Z. Sitar, J. Cryst. Growth 312, 58 (2009).

43 I. Bryan, A. Rice, L. Hussey, Z. Bryan, M. Bobea, S. Mita, J. Xie, R. Kirste, R. Collazo, and Z. Sitar, Appl. Phys. Lett. 102, 061602 (2013).

44 R. France, T. Xu, P. Chen, R. Chandrasekaran, and T.D. Moustakas, Appl. Phys. Lett. 90, 062115 (2007).

45 B.B. Haidet, B. Sarkar, P. Reddy, I. Bryan, Z. Bryan, R. Kirste, R. Collazo, and Z. Sitar, Jpn. J. Appl. Phys. 56, 100302 (2017).

46 J.L. Lyons, A. Janotti, and C.G. Van de Walle, Phys. Rev. B 89, 035204 (2014).

47 D. Alden, J.S. Harris, Z. Bryan, J.N. Baker, P. Reddy, S. Mita, G. Callsen, A. Hoffmann, D.L. Irving, R. Collazo, and Z. Sitar, Phys. Rev. Appl. 9, 054036 (2018).

48 J.S. Harris, J.N. Baker, B.E. Gaddy, I. Bryan, Z. Bryan, K.J. Mirrielees, P. Reddy, R. Collazo, Z. Sitar, and D.L. Irving, Appl. Phys. Lett. 112, 152101 (2018).

49 P. Reddy, F. Kaess, J. Tweedie, R. Kirste, S. Mita, R. Collazo, and Z. Sitar, Appl. Phys. Lett. 111, 152101 (2017).

50 D. Alden, J.S. Harris, Z. Bryan, J.N. Baker, P. Reddy, S. Mita, G. Callsen, A. Hoffmann, D.L. Irving, R. Collazo, and Z. Sitar, Phys. Rev. Appl. 9, 054036 (2018).

51 Q. Guo and A. Yoshida, Jpn. J. Appl. Phys. 33, 2453 (1994).

52 P. Reddy, I. Bryan, Z. Bryan, J. Tweedie, S. Washiyama, R. Kirste, S. Mita, R. Collazo, and Z. Sitar, Appl. Phys. Lett. 107, 091603 (2015).

53 P. Reddy, I. Bryan, Z. Bryan, W. Guo, L. Hussey, R. Collazo, and Z. Sitar, J. Appl. Phys. 116, 123701 (2014).

DISTRIBUTION A: Distribution approved for public release.

2.2 A Ge perspective on shallow doping in ultra-wide bandgap AlGaN

Background

Achieving controllable n-type doping in ultra-wide bandgap Al-rich AlGaN and AlN will lead to significant breakthroughs in optoelectronics, plasmonics, and high-voltage and high- power electronics.[1–4] Si and recently Ge have been utilized as shallow donors with low ionization energies (<30 meV) in GaN and AlGaN. Si remains a shallow donor in $Al_xGa_{1-x}N$ for x<0.8 and Ge for x<0.5,[5–9] with challenges primarily related to compensation due to impurities and vacancies.[10–15] Among the solutions to reduce compensation, simple optimizations of the growth conditions via temperature, gas flow, and pressure have been studied.[16–23] Further improvements were achieved by more advanced approaches involving defect formation energy manipulation via chemical potential and defect quasi Fermi level control methods.[24–27] However, when Al content exceeds 80% for Si (or equivalently 50% for Ge) an abrupt increase in the ionization energy of the donors is observed, associated with orders of magnitude lower carrier concentrations at room temperature.[5–9] The abrupt increase in the ionization energy has been attributed to the DX formation, as a result of relaxation of the donor to an off-site configuration.[5,7,28] The DX formation has been understood as a form of self-compensation that results in coexistence of d^+ shallow donor and DX^- acceptor, where the latter "pins" the bulk Fermi level deeper in the bandgap, resulting in a constant, low carrier concentration that is independent of doping. Consequently, within this model, the DX represents a fundamental upper limit to the free carrier concentration and conductivity in AlN and Al-rich AlGaN.

DX associated with a shallow to deep center transition with an increase in ionization energy was originally observed in the arsenide system in Te doped $Al_xGa_{1-x}As$ (x>0.22) and later for Si, Ge, and Sn doped AlGaAs. In those cases, the DX was observed to stabilize with increased Al composition and with hydrostatic pressure.[29–36] Similar to AlGaN, DX^{-1} in AlGaAs resulted in a reduction in carrier concentration and an increase in the ionization energy. To further understand the DX formation, the band structure of AlGaAs was examined. For the zincblende AlGaAs, either increasing the Al content or applying hydrostatic pressure[29] shifted all conduction band minima at Γ, L and X points in the first Brillouin zone to higher energies, albeit at different rates, with the highest change observed at Γ.[29] Consequently, above a certain Al composition (x~0.4) or an equivalent hydrostatic pressure, AlGaAs was no longer a direct bandgap semiconductor with Γ sub-band rising above the L and X sub-bands. Interestingly, the shallow donor configuration followed the Γ sub-band, resulting in a low ionization energy in Ga-rich, direct bandgap AlGaAs. However, the DX followed the average energy of the sub-bands and became more stable than the shallow donor state at higher Al-content or when hydrostatic pressure was applied.[29,31,37,38] Therefore, the DX formation appeared to be a shallow to deep level transformation of the substitutional donors induced by the relative changes in the conduction sub-band structure.[39] The Chadi and Chang model (CCM) was further employed to explain DX^{-1} formation of some donors in GaAs and AlGaAs.[40] Within this model, DX^{-1} is a localized deep state occupied by two electrons that repel each and can be stabilized by a large lattice relaxation with strong electron-phonon coupling and bond rupturing, resulting in local trigonal symmetry (C_{3v}).

In contrast to the arsenide system, shallow to deep transition for Si, Ge or O donors in AlGaN and AlN is not well understood. The nitrides exhibit a wurtzite crystal structure, and their band structure shows the conduction band minimum at Γ point for the entire compositional range (i.e., they retain the direct bandgap even at 100% Al content). However, a shallow to deep transition in $Al_xGa_{1-x}N$ was observed along with a sudden increase in the ionization energy (beyond that expected from the influence of the effective mass) from a few tens of meV to a few hundreds of meV when x exceeded 0.8, 0.5 and 0.4 for Si, Ge and O, respectively.[5,7,41] Mehnke et al. attributed the increased ionization energy of Si:AlGaN for compositions above 80% to the DX formation and identified the DX as an acceptor via EPR (electron paramagnetic resonance) studies.[42] Similarly, Zeisel et al. observed persistent photoconductivity (PPC) and an EPR signal in Si-doped AlN when illuminated by 1.3 eV light and concluded that the Si shallow donor was transitioning into a DX acceptor.[43] Son et al. employed temperature-dependent EPR studies in unintentionally Si doped AlN and found a DX^- configuration with an ionization energy of ~150 meV coexisting with on-site Si, which was behaving as a shallow donor.[44,45] Extending the DX studies to AlGaN, Trinh et al. and Nilsson

DISTRIBUTION A: Distribution approved for public release.

et al. concluded the beginning of the negative-U behavior for Si in $Al_xGa_{1-x}N$ (for x>0.77) by measuring temperature-dependent EPR, where the DX^- was concluded to form, but was very close to the shallow donor.[46,47] The DX^- was expected to shift away from the shallow donor with an increase in the Al composition, in agreement with theoretical studies.[48]

However, EPR identifies the DX^- once it is excited into the neutral shallow donor state with unpaired spin. In fact, Orlinskii et al. extended the EPR studies with ENDOR (electron-nuclear double resonance) spectra and identified singlet and triplet states of the shallow donor.[49] Hence, so far, the DX^{-1} identification has been indirect. In addition, the lack of the EPR signal at higher temperatures was attributed to either the diamagnetic character of the DX center or broadening of the EPR signal for highly localized defect centers and could not be used directly as a proof of DX^{-1} formation.[34,36] Moreover, elevated temperatures could change the electron occupancy and correspondingly the charge states of other point defects present in AlN whose effect could be recorded as a vanishing EPR signal. Based on EPR and C-V studies, Irmscher et al. proposed an alternative explanation of the high resistivity as compensation by deep acceptor traps with shallow acceptor traps at <1 eV from the conduction band as responsible for the high ionization energy for Si doped AlN.[50] Further, Skierbiszewski et al. performed pressure-dependent conductivity studies in Si-doped $Al_{0.58}Ga_{0.42}N$ and observed a DX-like behavior induced by pressure, but attributed a donor characteristic to it, which was contrary to the conventional acceptor DX configuration.[51]

Therefore, for donors in AlGaN and AlN, mainly the increase in the ionization energy along with observation of PPC and disappearance of the EPR signal by increasing temperatures were used in the literature to allude to the formation of a donor-related DX^{-1} state. However, the latter two observations are necessary conditions but not sufficient as evidence for the formation of the DX^{-1} state. PPC could arise due to macroscopic effects, such as interfaces, surfaces, or due to doping or compositional inhomogeneities, or due to microscopic effects, such as deep point defects acting as traps.[34,52,53] In addition, PPC has been observed also in GaN and low Al-content AlGaN, where DX^{-1} is not expected to be stable.[54,55]

Consequently, a more direct investigation of the charge state of the "DX" is necessary in III-nitrides. A more direct approach in determining the negative charge state (double electron occupancy) of the DX and its compensating nature can be achieved by co-doping. In this method, one of the dopants is a non-DX-forming shallow donor and the other is the donor whose transition into DX is to be studied. Measuring the concentration of dopants relative to the carrier concentration, the charge state of the DX may be determined.[32,39,56,57] Employing this method, Baj et al. confirmed the negative charge state of the Ge:DX in GaAs under hydrostatic pressure, where Ge was known to have a transition from a shallow donor to a deep state, hypothesized to be DX as determined by co-doping with Te, which remained a shallow donor under similar conditions.[56] Therefore, in zincblende arsenide system, donors were confirmed to undergo DX^{-1} transition above a certain Al composition (or a corresponding hydrostatic pressure).[57] Since Ge and Si in AlGaN undergo deep level transition at vastly different compositions (0.5 and 0.8, respectively), they are ideal to study the DX formation in AlGaN.[7] Hence, in this work, we used Si and Ge co-doped AlGaN of various compositions to track the electron occupancy of the Ge donor state.

Experimental

All AlGaN films were grown on c-oriented sapphire wafers in a vertical, low pressure (20 Torr), RF-heated MOCVD reactor with triethylgallium (TEG), trimethylaluminum (TMA), and ammonia as gallium, aluminum, and nitrogen precursors, respectively.[13] Prior to the low temperature AlN nucleation layer (20 nm) at 650°C, the sapphire substrate surface was exposed to H_2 at 1100°C for 7 min and in NH_3 ambient for nitridation at 950°C for 4 min. Then the nucleation layer was annealed at 1050°C for 15 minutes to obtain Al-polarity prior to the growth of a 100 nm thick high temperature AlN layer at 1200°C that served as an Al-polar AlN template. The AlN templates were annealed at the atmospheric pressure under N_2 for 1 hour at 1700°C to obtain low dislocation density (~10^9 cm^{-2}), as described elsewhere.[58] Subsequently, a 500 nm unintentionally doped AlN layer, followed by a 400 nm thick Ge doped or Ge and Si co-doped AlGaN layer, were grown. Germane and silane were used as the Ge and Si precursors, respectively. For Ge and Si co-doped samples, Si concentration was maintained constant at 1×10^{19} cm^{-3} while Ge concentration varied from undoped to 5×10^{19} cm^{-3}. The AlGaN layers were grown under H_2 diluent at 1100°C under 0.3 slm of

DISTRIBUTION A: Distribution approved for public release.

NH_3. An ION-TOF time-of-flight secondary ion mass spectrometer (TOF-SIMS) was used to determine the Ge and Si concentrations in AlGaN films. The acquisition conditions for the non-interlaced sputtering mode used for the measurement are described elsewhere.[59] Silicon and Germanium concentrations were determined under a negative ion detection mode and calibrated against an ion-implanted $Al_{0.3}Ga_{0.7}N$ standard. The aluminum/gallium ratio was also extracted from the SIMS data following the procedure explained elsewhere[60] and it agreed with the XRD measurements. The dislocation density in AlN template and AlGaN layers (~10^9 cm^{-2}), as well as AlGaN composition were determined by X-ray diffraction (XRD) using a Philips X'Pert materials research diffractometer with a Cu anode and using methods described elsewhere.[61] Ohmic contacts were realized on all AlGaN films by evaporation and rapid thermal annealing of V/Al/Ni/Au metal stacks at 850°C for 60s.[62] Electrical characterization was performed using a 8400 series LakeShore AC/DC Hall measurement system. Room temperature and temperature-dependent carrier concentration measurements were obtained under Van der Pauw configuration in a temperature range of 300-900 K.

Results and Discussion

The AlGaN compositions for this study were chosen to address three different scenarios for dopant configurations: (1) $Al_{0.4}Ga_{0.6}N$, where both Si and Ge behave as shallow donors that are almost fully ionized[13] at room temperature and the impurities assume the D^+ state, (2) $Al_{0.65}Ga_{0.35}N$, where Si behaves as a shallow donor (D^+) but Ge assumes a deep state (~150 meV),[6,7] which can be either the presumed DX^{-1} acceptor or a deep donor with negligible ionization at room temperature, i.e., D^0, as indicated by our previous work,[7] and (3) a transitional composition, $Al_{0.5}Ga_{0.5}N$, where Si behaves as a shallow donor but Ge transitions from the shallow state to a deep state and coexists in both configurations. As such, the Ge transitioning from the shallow state in $Al_{0.4}Ga_{0.6}N$ to a deep state in $Al_{0.65}Ga_{0.35}N$, while Si remains a shallow donor, allows for a direct identification of the Ge charge state. To minimize the influence of compensation, primarily C_N and V_{III} complexes, all AlGaN layers were grown with active compensation control using previously established techniques.[23,25]

In the first case, we study $Al_{0.4}Ga_{0.6}N$, where both Si and Ge are shallow donors.

Figure 1(a) shows the measured carrier concentration in $Al_{0.4}Ga_{0.6}N$ as a function of Ge concentration in the absence and presence of Si doping at 10^{19} cm^{-3}. Both Ge and Si act as shallow donors and the measured free electron concentration is approximately the sum of Si and Ge concentrations. Both dopants are fully ionized, and the compensation is negligible up to a Ge concentration of 2×10^{19} cm^{-3} (total dopant concentration of 3×10^{19} cm^{-3}). At higher Ge concentrations, self-compensation by the formation of V_{III}-nGe_{III} complexes suppresses further increase in the carrier concentration.[15] Figure 1 (b) shows the corresponding temperature-dependent carrier concentration for Si ($1x10^{19}$ cm^{-3}) doped $Al_{0.4}Ga_{0.6}N$ co-doped with Ge. As expected, a low ionization energy (less than 30 meV) is observed across the entire temperature range with no evidence of any deep states. The shallow donors are hydrogenic-like and their ionization energy depends only on the properties of the host lattice and is independent of the dopant. Therefore, both Ge and Si are in the D^+ state in $Al_{0.4}Ga_{0.6}N$.

DISTRIBUTION A: Distribution approved for public release.

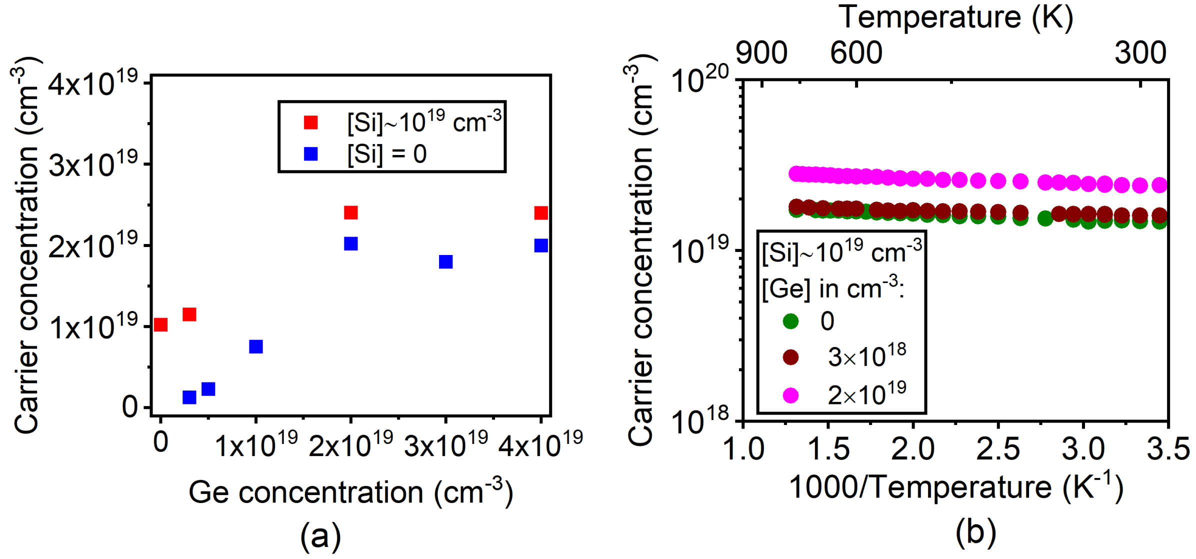

Figure 1: (a) RT free carrier concentration in $Al_{0.4}Ga_{0.6}N$ as a function of [Ge] in absence (blue) and presence of 10^{19} cm^{-3} Si (red); **(b)** Temperature-dependent carrier concentration for $Al_{0.4}Ga_{0.6}N$ co-doped with 10^{19} cm^{-3} Si different amounts of Ge.

In the second case, we study $Al_{0.65}Ga_{0.35}N$ where Si remains a shallow donor and Ge transitions to the deep state that is the subject of this study.[7]

Figure 2(a) shows the room temperature carrier concentration as a function of Ge concentration in presence and absence of Si ($1x10^{19}$ cm^{-3}). In absence of Si, Ge shows a typical "knee" behavior with carrier concentrations below 10^{17} cm^{-3} and ionization on the order of ~1%, for all doping levels. This corresponds to Ge occupying a deep state with an ionization energy of ~150 meV. In order to identify the nature of this deep state, the samples were co-doped with a verified shallow donor, Si. As expected, a Si-doped sample without Ge, showed a carrier concentration corresponding to the Si concentration of ~10^{19} cm^{-3}. Practically full ionization of Si shifts the Fermi level in AlGaN close to the conduction band.

When Ge is added to this n-type system, one expects two different outcomes corresponding to the Ge being in the neutral D^0 or DX^{-1} acceptor state.[28] If Ge behaves as a neutral deep donor, it will not attract electrons from the conduction band and, thus, adding Ge to a Si-doped sample is not expected to change free carrier concentration. In contrast, if Ge forms a negatively charged DX^{-1} acceptor state, the carrier concentration of the Si-doped samples should decrease as each Ge captures a free electron to form a negative acceptor state. Therefore, a sudden drop in the carrier concentration is expected with the Ge concentration reaches the Si concentration. As shown in Figure 2(b), the free electron concentration should decrease with [Ge] based on the charge balance equation as follows:

$$n = [Si] - \frac{[Ge]}{1 + g_A \exp(\frac{E_A - E_f}{k_B T})} \tag{1}$$

where g_A is the degeneracy factor, E_A is the energy level of the Ge acceptor state, and E_F is the Fermi level. Equation (1) assumes negligible compensation, which is reasonable for all total dopant concentrations below ~$3x10^{19}$ cm^{-3}. For the calculations, the ionization energy is assumed to be 150 meV as measured previously.[7] The expected carrier concentration for the two scenarios is depicted in Figure 2 (b).

As shown in Figure 2(a), co-doping of Si-doped $Al_{0.65}Ga_{0.35}N$ with Ge resulted in practically constant electron concentrations for a wide range of Ge concentrations. Hence, comparing Figures 2(a) and 2(b), we may conclude that Ge in $Al_{0.65}Ga_{0.35}N$ has to be in a neutral deep donor state and not in a negative DX^- acceptor state, as the latter should have resulted in negligible free carrier concentration once the [Ge]

DISTRIBUTION A: Distribution approved for public release.

surpassed [Si]. Interestingly, beyond the knee concentration of Ge, where it is expected to self-compensate by forming complexes with V_{III}[15] accounting for the minor decrease in free carrier concentration as shown in Figure 2(a), which is related to V_{III}-nGe_{III} complex formation; the "knee" in Figure 2(a) is consistent with Figure 1, and previous studies of heavily doped samples.[15]

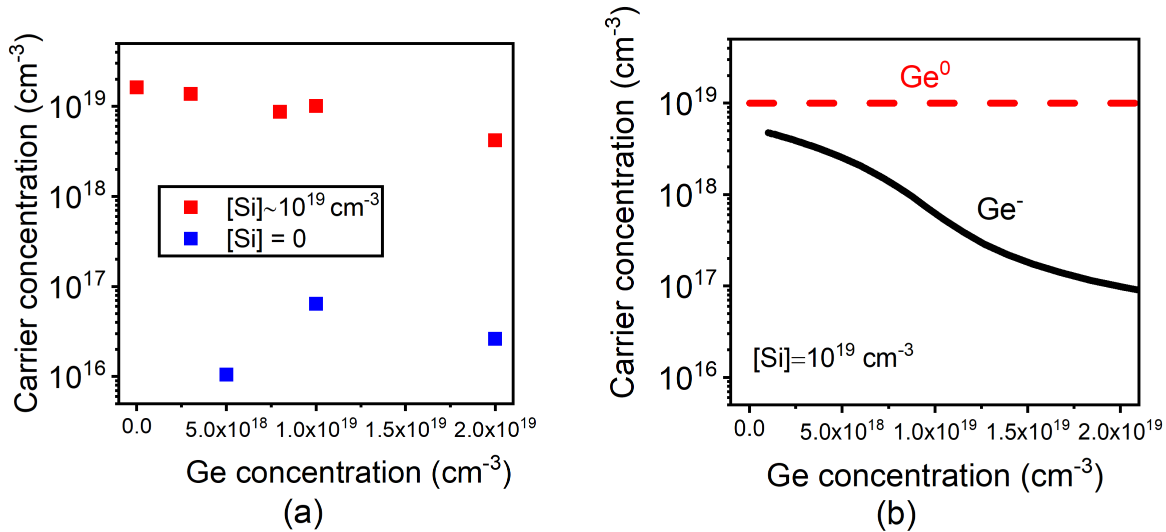

Figure 2: (a) RT free carrier concentration in $Al_{0.65}Ga_{0.35}N$ as a function of [Ge] in absence (blue) and presence of 10^{19} cm^{-3} Si (red); **(b)** Free carrier concentration as a function [Ge] in Si-doped $Al_{0.65}Ga_{0.35}N$, calculated from Equation (1) for Ge^0 (red) and Ge^{-1} (black).

Figure 3 (a) shows the free carrier concentration as a function of temperature in Si-doped (10^{19} cm^{-3}) $Al_{0.65}Ga_{0.35}N$ co-doped with various amounts of Ge. In the absence of Ge, Si behaves as a shallow donor with low ionization energy (< 30 meV) over the entire studied temperature range of 300–900 K. However, all Si and Ge co-doped AlGaN layers show a second donor that is ionized at higher temperatures, i.e., a deep donor with a higher ionization energy corresponding to the Ge deep donor state. This Ge donor is neutral at room temperature and does not affect neither the Fermi level nor the carrier concentration, due to its high activation energy. However, it is ionized at elevated temperatures, resulting in an increase in free carrier concentration beyond the [Si], as shown in Figure 3 (a). This is possible only by the presence of a deep donor and not for an acceptor state, as shown in Figure 3 (b), where Ge acting as a deep acceptor shows a single high ionization energy corresponding to the energy barrier between the DX^{-1} and d^+. The presence of two ionization energies (two slopes) is not predicted considering the charge balance equation for Ge acting as DX^{-1}, and is exclusively a signature of two donors. Hence, Ge exhibits a deep (0/+) donor type thermodynamic transition rather than a (+/-) transition as suggested by prior work.[7]

DISTRIBUTION A: Distribution approved for public release.

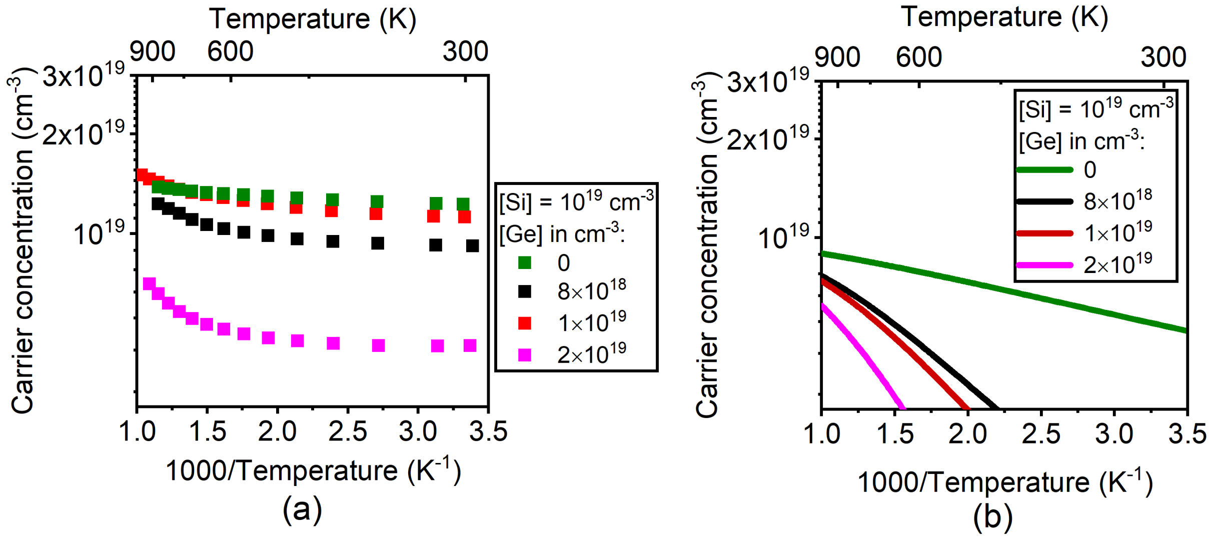

Figure 3: (a) Temperature-dependent free carrier concentration in $Al_{0.65}Ga_{0.35}N$ as a co-doped with constant [Si] of ~1×10^{19} cm^{-3} and variable [Ge]. **(b)** Calculated temperature-dependent free carrier concentration simulating doping concentration in Figure 3 (a) but assuming coexistence of Ge^{-1} and Si^{+}. Notably, the expected behavior is completely different from the experimental data.

In Figure 4, we study the transition of Ge from shallow to deep donor as a function of alloy composition. For all compositions, Ge and Si concentrations are kept constant at ~8×10^{18} cm^{-3} and ~1×10^{19} cm^{-3}, respectively. All other impurities are at least one order of magnitude lover level due to the active management of compensators during growth.[12,63] Figure 4(a) indicates the expected carrier concentrations for Ge in d^{+}, D^{0} and DX^{-} states. While dopant concentrations remain constant, the increase in the Al content causes a reduction in the room temperature carrier concentration. The corresponding reduction is approximately equal to the Ge concentration, as expected from its transition to a deep donor. In contrast, a reduction in carrier concentration twice that of the Ge concentration was observed for previously in GaAs co-doped with Te and Ge where Ge was in a DX^{-1} state.[56] At higher temperatures, the difference in carrier concentrations decreases due to the partial ionization of the deep Ge donor. Interestingly, in $Al_{0.5}Ga_{0.5}N$, a distribution of shallow and deep Ge donor states is observed where at higher temperatures almost full ionization of the donors is witnessed. In contrast, in $Al_{0.4}Ga_{0.6}N$, both Ge and Si are shallow donors. As for $Al_{0.65}Ga_{0.4}N$, Si is a shallow donor and Ge is a deep donor.

The change of carrier concentration with temperature for the same samples grown at different Al contents is shown in Figure 4(b). In $Al_{0.4}Ga_{0.6}N$, one single ionization energy (<30 meV) is observed, indicating that Ge and Si are both shallow donors with similar ionization energies. On the other hand, $Al_{0.65}Ga_{0.4}N$ shows two ionization energies (two slopes), one for shallow Si and one for deep Ge donor. $Al_{0.5}Ga_{0.5}N$ exhibits the two ionization energies as well and shows a saturation of carriers at higher temperatures, indicating a full ionization of deep Ge donors occurs, as expected.

DISTRIBUTION A: Distribution approved for public release.

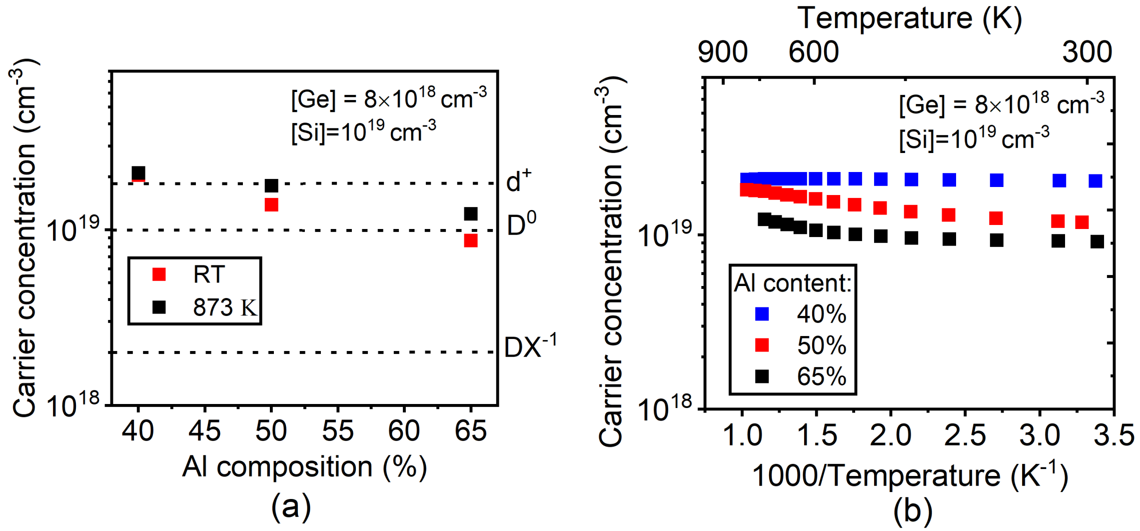

Figure 4: (a) Free carrier concentration as a function of AlGaN composition for co-doped samples (Si ~ 10^{19} cm^{-3} and Ge ~ 8×10^{18} cm^{-3}) at RT and 900 K. (b) Temperature dependent carrier concentration of samples in Figure 4 (a).

The observation of Ge as a deep donor requires a revision of the models proposed to explain donor states in Al-rich AlGaN and AlN.[43] This work shows that Ge in $Al_{0.65}Ga_{0.35}N$ is neutral with a (0/+) thermodynamic transition. Consequently, the deep donor state should exhibit a Ge_{III} configuration with a relatively small lattice displacement or relaxation. This makes the DX^{-1} state with large lattice relaxation and bond rupturing unstable. As such, the deep donor state with an ionization energy of 150 meV is the most stable state in $Al_xGa_{1-x}N$ for x>0.6.

The co-doping experiment is a direct proof of the Ge transition to a deep donor in AlGaN. It could suggest a similar behavior for other donors, such as Si, and O. Recently a similar distribution of shallow and deep states was reported in Si-implanted AlN, supporting the expectation of a similar behavior for other donors in Al-rich AlGaN and AlN.[64] As discussed in the introduction, the DX formation is dependent on the energy shifts of the various Brillouin zone critical points that determine the conduction band minima as a function of alloy composition and pressure. As such, there exists a contrasting behavior between the arsenide systems with a cubic crystal structure and the nitride systems with a wurtzite crystal system. This finding has profound technological consequences: while the DX formation caps the achievable free carrier concentration a very low level, deep donor formation allows for technologically relevant conductivity. This should inspire additional theoretical studies to understand the nature of the shallow to deep donor transitions in these ultra-wide bandgap semiconductors.

Conclusion

In conclusion, Ge and Si co-doping experiments were used in $Al_xGa_{1-x}N$ ($0.4<x<0.65$) to establish the electron occupancy of the Ge state in AlGaN. Both Ge and Si acted as shallow donors in $Al_{0.4}Ga_{0.6}N$, exhibiting a single, low ionization energy and practically complete ionization. However, in Ge-doped $Al_{0.65}Ga_{0.35}N$, carrier concentrations at room temperature were orders of magnitude lower than [Ge]. Co-doping with Si, which served as a source of free electrons, revealed that Ge was neutral at room temperature (neither generating electrons nor causing compensation); at elevated temperatures, Ge behaved as a donor with high ionization energy. No DX^{-1} with a (+/-) thermodynamic transition was observed. Ge as a deep donor with (0/+) thermodynamic transition was the most stable state in the band; Si is expected to behave similarly. This is contrary to the AlGaAs system, where the donor-related DX^{-1} was previously proven to be the stable state in AlGaAs (or GaAs under hydrostatic pressure) based on the Chadi-Chang model. The different behavior of the donors may stem from the basic differences in the arsenide and III-nitride crystal systems and corresponding band structures. The fact that the neutral deep donors are the most stable states (rather than the negatively charged acceptor states) creates a great opportunity in III-nitrides as there are no

DISTRIBUTION A: Distribution approved for public release.

intrinsic limitations in n-type doping of these ultra-wide bandgap semiconductors. This should allow for technologically-relevant n-type conductivity in Al-rich AlGaN and AlN for applications in optoelectronics and electronics.

References

1 Y. Taniyasu, M. Kasu, and T. Makimoto, Nat. Lond. 441, 325 (2006).

2 K. Ban, J. Yamamoto, K. Takeda, K. Ide, M. Iwaya, T. Takeuchi, S. Kamiyama, I. Akasaki, and H. Amano, Appl. Phys. Express 4, 052101 (2011).

3 J.Y. Tsao, S. Chowdhury, M.A. Hollis, D. Jena, N.M. Johnson, K.A. Jones, R.J. Kaplar, S. Rajan, C.G.V. de Walle, E. Bellotti, C.L. Chua, R. Collazo, M.E. Coltrin, J.A. Cooper, K.R. Evans, S. Graham, T.A. Grotjohn, E.R. Heller, M. Higashiwaki, M.S. Islam, P.W. Juodawlkis, M.A. Khan, A.D. Koehler, J.H. Leach, U.K. Mishra, R.J. Nemanich, R.C.N. Pilawa-Podgurski, J.B. Shealy, Z. Sitar, M.J. Tadjer, A.F. Witulski, M. Wraback, and J.A. Simmons, Adv. Electron. Mater. 4, 1600501 (2018).

4 P. Bagheri, P. Reddy, J.H. Kim, R. Rounds, T. Sochacki, R. Kirste, M. Bockowski, R. Collazo, and Z. Sitar, Appl. Phys. Lett. 117, 082101 (2020).

5 R. Collazo, S. Mita, J. Xie, A. Rice, J. Tweedie, R. Dalmau, and Z. Sitar, Phys. Status Solidi C 8, 2031 (2011).

6 A. Bansal, K. Wang, J.S. Lundh, S. Choi, and J.M. Redwing, Appl. Phys. Lett. 114, 142101 (2019).

7 P. Bagheri, R. Kirste, P. Reddy, S. Washiyama, S. Mita, B. Sarkar, R. Collazo, and Z. Sitar, Appl. Phys. Lett. 116, 222102 (2020).

8 M.L. Nakarmi, K.H. Kim, K. Zhu, J.Y. Lin, and H.X. Jiang, Appl. Phys. Lett. 85, 3769 (2004).

9 B. Borisov, V. Kuryatkov, Yu. Kudryavtsev, R. Asomoza, S. Nikishin, D.Y. Song, M. Holtz, and H. Temkin, Appl. Phys. Lett. 87, 132106 (2005).

10 F. Kaess, S. Mita, J. Xie, P. Reddy, A. Klump, L.H. Hernandez-Balderrama, S. Washiyama, A. Franke, R. Kirste, A. Hoffmann, R. Collazo, and Z. Sitar, J. Appl. Phys. 120, 105701 (2016).

11 J.S. Harris, J.N. Baker, B.E. Gaddy, I. Bryan, Z. Bryan, K.J. Mirrielees, P. Reddy, R. Collazo, Z. Sitar, and D.L. Irving, Appl. Phys. Lett. 112, 152101 (2018).

12 S. Washiyama, P. Reddy, B. Sarkar, M.H. Breckenridge, Q. Guo, P. Bagheri, A. Klump, R. Kirste, J. Tweedie, S. Mita, Z. Sitar, and R. Collazo, J. Appl. Phys. 127, 105702 (2020).

13 I. Bryan, Z. Bryan, S. Washiyama, P. Reddy, B. Gaddy, B. Sarkar, M.H. Breckenridge, Q. Guo, M. Bobea, J. Tweedie, S. Mita, D. Irving, R. Collazo, and Z. Sitar, Appl. Phys. Lett. 112, 062102 (2018).

14 S.F. Chichibu, H. Miyake, Y. Ishikawa, M. Tashiro, T. Ohtomo, K. Furusawa, K. Hazu, K. Hiramatsu, and A. Uedono, J. Appl. Phys. 113, 213506 (2013).

15 S. Washiyama, K.J. Mirrielees, P. Bagheri, J.N. Baker, J.-H. Kim, Q. Guo, R. Kirste, Y. Guan, M.H. Breckenridge, A.J. Klump, P. Reddy, S. Mita, D.L. Irving, R. Collazo, and Z. Sitar, Appl. Phys. Lett. 118, 042102 (2021).

16 K. Ikenaga, A. Mishima, Y. Yano, T. Tabuchi, and K. Matsumoto, Jpn. J. Appl. Phys. 55, 05FE04 (2016).

17 T. Tanikawa, S. Kuboya, and T. Matsuoka, Phys. Status Solidi B 254, n/a (2017).

18 S. Mita, R. Collazo, A. Rice, R.F. Dalmau, and Z. Sitar, J. Appl. Phys. 104, 013521 (2008).

19 C. Lund, S. Nakamura, S.P. DenBaars, U.K. Mishra, and S. Keller, J. Cryst. Growth 464, 127 (2017).

20 N.A. Fichtenbaum, T.E. Mates, S. Keller, S.P. DenBaars, and U.K. Mishra, J. Cryst. Growth 310, 1124 (2008).

21 A.M. Armstrong, M.W. Moseley, A.A. Allerman, M.H. Crawford, and J.J. Wierer, J. Appl. Phys. 117, 185704 (2015).

22 D.D. Koleske, A.E. Wickenden, R.L. Henry, and M.E. Twigg, J. Cryst. Growth 242, 55 (2002).

23 F. Kaess, S. Mita, J. Xie, P. Reddy, A. Klump, L.H. Hernandez-Balderrama, S. Washiyama, A. Franke, R. Kirste, A. Hoffmann, R. Collazo, and Z. Sitar, J. Appl. Phys. 120, 105701 (2016).

24 P. Reddy, M.P. Hoffmann, F. Kaess, Z. Bryan, I. Bryan, M. Bobea, A. Klump, J. Tweedie, R. Kirste, S. Mita, M. Gerhold, R. Collazo, and Z. Sitar, J. Appl. Phys. 120, 185704 (2016).

25 P. Reddy, F. Kaess, J. Tweedie, R. Kirste, S. Mita, R. Collazo, and Z. Sitar, Appl. Phys. Lett. 111, 152101 (2017).

26 P. Reddy, S. Washiyama, F. Kaess, R. Kirste, S. Mita, R. Collazo, and Z. Sitar, J. Appl. Phys. 122, 245702 (2017).

DISTRIBUTION A: Distribution approved for public release.

27 S. Washiyama, P. Reddy, B. Sarkar, M.H. Breckenridge, Q. Guo, P. Bagheri, A. Klump, R. Kirste, J. Tweedie, S. Mita, Z. Sitar, and R. Collazo, J. Appl. Phys. 127, 105702 (2020).

28 L. Gordon, J.L. Lyons, A. Janotti, and C.G. Van de Walle, Phys. Rev. B 89, 085204 (2014).

29 P.M. Mooney, J. Appl. Phys. 67, R1 (1990).

30 D.V. Lang, R.A. Logan, and M. Jaros, Phys. Rev. B 19, 1015 (1979).

31 N. Lifshitz, A. Jayaraman, R.A. Logan, and H.C. Card, Phys. Rev. B 21, 670 (1980).

32 T. Fujisawa, J. Yoshino, and H. Kukimoto, 6 (n.d.).

33 P.M. Mooney, Radiat. Eff. Defects Solids 111–112, 281 (1989).

34 J.E. Dmochowski, L. Dobaczewski, J.M. Langer, and W. Jantsch, Phys. Rev. B 40, 9671 (1989).

35 W. Shan, P.Y. Yu, M.F. Li, W.L. Hansen, and E. Bauser, Phys. Rev. B 40, 7831 (1989).

36 K. Khachaturyan, E.R. Weber, and M. Kaminska, Mater. Sci. Forum 38–41, 1067 (1991).

37 M. Zazoui, S.L. Feng, and J.C. Bourgoin, Phys. Rev. B 41, 8485 (1990).

38 T. Suski, Mater. Sci. Forum 143–147, 975 (1993).

39 P.Y. Yu and M. Cardona, Fundamentals of Semiconductors: Physics and Materials Properties, 4th ed (Springer, Berlin ; New York, 2010).

40 D.J. Chadi and K.J. Chang, Phys. Rev. B 39, 10063 (1989).

41 C. Wetzel, T. Suski, J.W. Ager III, E.R. Weber, E.E. Haller, S. Fischer, B.K. Meyer, R.J. Molnar, and P. Perlin, Phys. Rev. Lett. 78, 3923 (1997).

42 F. Mehnke, X.T. Trinh, H. Pingel, T. Wernicke, E. Janzén, N.T. Son, and M. Kneissl, J. Appl. Phys. 120, 145702 (2016).

43 R. Zeisel, M.W. Bayerl, S.T.B. Goennenwein, R. Dimitrov, O. Ambacher, M.S. Brandt, and M. Stutzmann, Phys. Rev. B 61, R16283 (2000).

44 N.T. Son, M. Bickermann, and E. Janzén, Phys. Status Solidi C 8, 2167 (2011).

45 N.T. Son, M. Bickermann, and E. Janzén, Appl. Phys. Lett. 98, 092104 (2011).

46 X. Thang Trinh, D. Nilsson, I.G. Ivanov, E. Janzén, A. Kakanakova-Georgieva, and N. Tien Son, Appl. Phys. Lett. 103, 042101 (2013).

47 D. Nilsson, X.T. Trinh, E. Janzén, N.T. Son, and A. Kakanakova-Georgieva, Phys. Status Solidi B 252, 1306 (2015).

48 L. Gordon, J.L. Lyons, A. Janotti, and C.G. Van de Walle, Phys. Rev. B 89, 085204 (2014).

49 S.B. Orlinskii, J. Schmidt, P.G. Baranov, M. Bickermann, B.M. Epelbaum, and A. Winnacker, Phys. Rev. Lett. 100, 256404 (2008).

50 K. Irmscher, T. Schulz, M. Albrecht, C. Hartmann, J. Wollweber, and R. Fornari, Phys. B Condens. Matter 401–402, 323 (2007).

51 C. Skierbiszewski, T. Suski, M. Leszczynski, M. Shin, M. Skowronski, M.D. Bremser, and R.F. Davis, Appl. Phys. Lett. 74, 3833 (1999).

52 H.J. von Bardeleben, I. Buyanova, A. Belyaev, and M. Sheinkman, Phys. Rev. B 45, 11667 (1992).

53 N.G. Semaltianos, G. Karczewski, B. Hu, T. Wojtowicz, and J.K. Furdyna, Phys. Rev. B 51, 17499 (1995).

54 M.T. Hirsch, J.A. Wolk, W. Walukiewicz, and E.E. Haller, Appl. Phys. Lett. 71, 1098 (1997).

55 J.Z. Li, J.Y. Lin, H.X. Jiang, M. Asif Khan, and Q. Chen, J. Appl. Phys. 82, 1227 (1997).

56 M. Baj, L.H. Dmowski, and T. Słupiński, Phys. Rev. Lett. 71, 3529 (1993).

57 M.-F. Li and P.Y. Yu, Jpn. J. Appl. Phys. 32, 200 (1993).

58 S. Washiyama, Y. Guan, S. Mita, R. Collazo, and Z. Sitar, J. Appl. Phys. 127, 115301 (2020).

59 A. Klump, C. Zhou, F.A. Stevie, R. Collazo, and Z. Sitar, J. Vac. Sci. Technol. B Nanotechnol. Microelectron. Mater. Process. Meas. Phenom. 36, 03F102 (2018).

60 C.J. Gu, F.A. Stevie, C.J. Hitzman, Y.N. Saripalli, M. Johnson, and D.P. Griffis, Appl. Surf. Sci. 252, 7228 (2006).

61 J. Tweedie, R. Collazo, A. Rice, J. Xie, S. Mita, R. Dalmau, and Z. Sitar, J. Appl. Phys. 108, 043526 (2010).

DISTRIBUTION A: Distribution approved for public release.

62 B.B. Haidet, B. Sarkar, P. Reddy, I. Bryan, Z. Bryan, R. Kirste, R. Collazo, and Z. Sitar, Jpn. J. Appl. Phys. 56, 100302 (2017).

63 P. Reddy, S. Washiyama, F. Kaess, R. Kirste, S. Mita, R. Collazo, and Z. Sitar, J. Appl. Phys. 122, 245702 (2017).

64 M. Hayden Breckenridge, Q. Guo, A. Klump, B. Sarkar, Y. Guan, J. Tweedie, R. Kirste, S. Mita, P. Reddy, R. Collazo, and Z. Sitar, Appl. Phys. Lett. 116, 172103 (2020).

DISTRIBUTION A: Distribution approved for public release.

2.3 List of publications acknowledging AFOSR support under FA9550-17-1-0225 (total 32)

1. *Mirrielees KJ, Dycus JH, Baker JN, Reddy P, Collazo R, Sitar Z, LeBeau JM, Irving DL, “Native oxide reconstructions on AlN and GaN (0001) surfaces,” Journal of Applied Physics 129, 195304 (2021).
2. Breckenridge HM, Bagheri P, Guo Q, Sarkar B, Khachariya D, Pavlidis S, Tweedie J, Kirste R, Mita S, Reddy P, Collazo R, Sitar Z, “High n-type conductivity and carrier concentration in Si-implanted homoepitaxial AlN,” Applied Physics Letters 118, 112104 (2021).
3. Al-Tawhid A, Shafe A-A, Bagheri P, Guan Y, Reddy P, Mita S, Moody B, Collazo R, Sitar Z, Ahadi K, “Weak localization and dimensional crossover in compositionally graded $Al_xGa_{1-x}N$,” Applied Physics Letters 118, 082101 (2021).
4. Washiyama S, Mirrielees KJ, Bagheri P, Baker JN, Kim J-H, Guo Q, Kirste R, Guan Y, Breckenridge MH, Klump AJ, Reddy P, Mita S, Irving DL, Collazo R, Sitar Z, “Self-compensation in heavily Ge doped AlGaN: A comparison to Si doping,” Applied Physics Letters 118, 042102 (2021).
5. Breckenridge HM, Tweedie J, Reddy P, Guan Y, Bagheri P, Szymanski P, Mita S, Sierakowski K, Boćkowski M, Collazo R, Sitar Z, “High Mg activation in implanted GaN by high temperature and ultrahigh pressure annealing,” Applied Physics Letters 118, 022101 (2021).
6. Baker JN, Bowes PC, Harris JS, Collazo R, Sitar Z, Irving DL, “Complexes and compensation in degenerately donor doped GaN,” Applied Physics Letters 117, 102109 (2020).
7. Hauwiller MR, Stowe D, Eldred TB, Mita S, Collazo R, Sitar Z, LeBeau J, “Cathodoluminescence of silicon doped aluminum nitride with scanning transmission electron microscopy,” APL Materials 8, 091110 (2020).
8. Vetter E, Biliroglu M, Seyitliyev D, Reddy P, Kirste R, Sitar Z, Collazo R, Gundogdu K, Sun D, “Observation of carrier concentration dependent spintronic terahertz emission from n-GaN/NiFe heterostructures,” Applied Physics Letters 117, 093502 (2020).
9. Bagheri P, Reddy P, Kim JH, Rounds R, Sochacki T, Kirste R, Bockowski M, Collazo R, Sitar Z, “Impact of impurity-based phonon resonant scattering on thermal conductivity of single crystalline GaN,” Applied Physics Letters 117, 082101 (2020).
10. Khachariya D, Szymanski D, Sengupta R, Reddy P, Kohn E, Sitar Z, Collazo R, Pavlidis S, “Chemical treatment effects on Schottky contacts to metalorganic chemical vapor deposited n-type N-polar GaN,” Journal of Applied Physics 128, 064501, (2020).
11. Qiang Guo Q, Ronny Kirste R, Pramod Reddy P, Will Mecouch W, Yan Guan Y, Seiji Mita S, Shun Washiyama S, James Tweedie J, Zlatko Sitar Z, Ramón Collazo R, “Impact of the effective refractive index in AlGaN-based mid-UV laser structures on waveguiding,” Japanese Journal of Applied Physics 59, 091001 (2020).
12. Bagheri P, Kirste R, Reddy P, Washiyama S, Mita S, Sarkar B, Collazo R, Sitar Z, “The nature of the DX state in Ge-doped AlGaN,” Applied Physics Letters 116, 222102 (2020).
13. Breckenridge HM, Guo Q, Klump A, Sarkar B, Guan Y, Tweedie J, Kirste R, Mita S, Reddy P, Collazo R, Sitar Z, “Shallow Si donor in ion-implanted homoepitaxial AlN,” Applied Physics Letters 116, 172103 (2020).
14. Reddy P, Khachariya D, Szymanski D, Breckenridge MH, Sarkar B, Pavlidis S, Collazo R, Sitar Z, Kohn E, “Role of polarity in SiN on Al/GaN and the pathway to stable contacts,” Semiconductor Science and Technology 35, 055007 (2020).
15. Washiyama S, Guan Y, Mita S, Collazo R, Sitar Z, “Recovery kinetics in high temperature annealed AlN heteroepitaxial films,” Journal of Applied Physics 127, 115301 (2020).
16. Washiyama S, Reddy P, Sarkar B, Breckenridge MH, Guo Q, Bagheri P, Klump A, Kirste R, Tweedie J, Mita S, Sitar Z, Collazo R, “The role of chemical potential in compensation control in Si:AlGaN,” Journal of Applied Physics 127 (10), 105702, (2020).
17. Reddy P, Breckenridge MH, Guo Q, Klump A, Khachariya D, Pavlidis S, Mecouch W, Mita S, Moody B, Tweedie J, Kirste R, Kohn E, Collazo R, Sitar Z, “High gain, large area, and solar blind avalanche photodiodes based on Al-rich AlGaN grown on AlN substrates,” Applied Physics Letters 116, 081101 (2020).
18. Reddy P, Khachariya D, Szymanski D, Breckenridge MH, Sarkar B, Pavlidis S, Collazo R, Sitar Z, Kohn, E, “Role of polarity in SiN on Al/GaN and the pathway to stable contacts,” Semiconductor Science and Technology 35, 055007 (2020).

DISTRIBUTION A: Distribution approved for public release.

19. Klump A, Hoffmann MP, Kaess F, Tweedie J, Reddy P, Kirste R, Sitar Z, Collazo R, "Control of passivation and compensation in Mg-doped GaN by defect quasi Fermi level control," Journal of Applied Physics 127, 045702 (2020).
20. Reddy P, Bryan Z, Bryan I, Kim JH, Washiyama S, Kirste R, Mita S, Tweedie J, Irving DL, Collazo R, Sitar Z, "Pinning of energy transitions of defects, complexes, and surface states in AlGaN alloys," Applied Physics Letters 116, 032102 (2020).
21. Guo Q, Kirste R, Mita S, Tweedie J, Reddy P, Moody B, et al. Design of AlGaN-based quantum structures for low threshold UVC lasers. Journal of Applied Physics. 2019;126(22):223101.
22. Kirste R, Mita S, Reddy P, Franke A, Guo Q, Wang K, et al. Development of Near UV Laser Diodes. In 2019. p. 1–3.
23. Reddy P, Breckenridge MH, Klump A, Guo Q, Mita S, Sarkar B, et al. Al Rich AlGaN Based APDs on Single Crystal AlN with Solar Blindness and Room Temperature Operation. In 2019. p. 1–3.
24. Guo Q, Kirste R, Reddy P, Mita S, Guan Y, Collazo R, et al. Quantum Well-Width Dependence Study on AlGaN Based UVC Laser. In 2019. p. 1–4.
25. Guo Q, Kirste R, Mita S, Tweedie J, Reddy P, Washiyama S, et al. The polarization field in Al-rich AlGaN multiple quantum wells. Japanese Journal of Applied Physics. 2019 May 9;58(SC):SCCC10.
26. Bobea Graziano M, Bryan I, Bryan Z, Kirste R, Tweedie J, Collazo R, et al. Structural characteristics of m-plane AlN substrates and homoepitaxial films. Journal of Crystal Growth. 2019 Feb 1;507:389–94.
27. Dycus JH, Washiyama S, Eldred TB, Guan Y, Kirste R, Mita S, et al. The role of transient surface morphology on composition control in AlGaN layers and wells. Applied Physics Letters. 2019;114(3):031602.
28. Reddy P, Washiyama S, Mecouch W, Hernandez-Balderrama LH, Kaess F, Breckenridge MH, et al. Plasma enhanced chemical vapor deposition of SiO2 and SiNx on AlGaN: Band offsets and interface studies as a function of Al composition. Journal of Vacuum Science & Technology A. 2018;36(6):061101.
29. Rounds R, Sarkar B, Sochacki T, Bockowski M, Imanishi M, Mori Y, et al. Thermal conductivity of GaN single crystals: Influence of impurities incorporated in different growth processes. Journal of Applied Physics. 2018;124(10):105106.
30. Rounds R, Sarkar B, Alden D, Guo Q, Klump A, Hartmann C, et al. The influence of point defects on the thermal conductivity of AlN crystals. Journal of Applied Physics. 2018;123(18):185107.
31. Rounds R, Sarkar B, Klump A, Hartmann C, Nagashima T, Kirste R, et al. Thermal conductivity of single-crystalline AlN. Applied Physics Express. 2018;11(7):071001.
32. Bryan I, Bryan Z, Washiyama S, Reddy P, Gaddy B, Sarkar B, et al. Doping and compensation in Al-rich AlGaN grown on single crystal AlN and sapphire by MOCVD. Applied Physics Letters. 2018;112(6):062102.

DISTRIBUTION A: Distribution approved for public release.